SELF-SUPERVISED TEMPORAL SUPER RESOLUTION OF ENERGY DATA USING GENERATIVE ADVERSARIAL TRANSFORMERS

Xuanhao Mu, Gökhan Demirel, Yuzhe Zhang, Jianlei Liu, Thorsten Schlachter and Veit Hagenmeyer
Institute for Automation and Applied Informatics (IAI)
Karlsruhe Institute of Technology
76344 Eggenstein-Leopoldshafen, Germany
xuanhao.mu@kit.edu goekhan.demirel@kit.edu yuzhe.zhang@student.kit.edu
jianlei.liu@kit.edu thorsten.schlachter@kit.edu veit.hagenmeyer@kit.edu

ABSTRACT

To bridge the temporal granularity gap in energy network design and operation based on Energy System Models, resampling of time series is required. While conventional upsampling methods are computationally efficient, they often result in significant information loss or increased noise. Advanced models such as time series generation models, Super-Resolution models and imputation models show potential, but also face fundamental challenges. The goal of time series generative models is to learn the distribution of the original data to generate high-resolution series with similar statistical characteristics. This is not entirely consistent with the definition of upsampling. Time series Super-Resolution models or imputation models can degrade the accuracy of upsampling because the input low-resolution time series are sparse and may have insufficient context. Moreover, such models usually rely on supervised learning paradigms. This presents a fundamental application paradox: their training requires the high-resolution time series that is intrinsically absent in upsampling application scenarios. To address the mentioned upsampling issue, this paper introduces a new method utilizing Generative Adversarial Transformers (GATs), which can be trained without access to any ground-truth high-resolution data. Compared with conventional interpolation methods, the introduced method can reduce the root mean square error (RMSE) of upsampling tasks by 9%, and the accuracy of a model predictive control (MPC) application scenario is improved by 13%.

***K*eywords** Transformer, Generative Adversarial Network, Granularity Gap, Super Resolution, Smart Energy

1 Introduction

In recent years, the question of how energy systems can be decarbonized has received increasing attention due to global climate change and rising carbon dioxide emissions [1]. Energy System Models (ESMs) analyze energy system decarbonization pathways through mathematical modeling and simulation. Due to the complexity of these systems, multiple models often need to be coupled for joint analysis [2]. However, these independent models must compress the representation of temporal, spatial, or technological information for computational complexity reasons, leading to a loss of precision known as the granularity gap [3]. One direct consequence of this gap is that different models participating in joint simulations often run at their own inherent time resolutions. For instance, combining an electrical grid model (with a 15-minute resolution) with a gas network model (with an hourly resolution) creates temporal mismatches. Poncelet et al. [4] noted that choosing time series with different temporal resolutions can affect the simulation results. Therefore, accurately interpolating time-series data is essential for robust model coupling.

Researchers typically use conventional methods such as linear interpolation. These methods are simple and computationally efficient, but often fail to capture the complex nonlinear features inherent in data and tend to introduce noise. Advanced machine learning models such as time series generation models, Super-Resolution (SR) models and imputation models present viable alternatives but encounter inherent difficulties. Time series generation models aim to learn data distributions to create new sequences. SR aims to establish an accurate mapping from low-resolution to high-resolution sequences, while imputation is a more general approach for filling in missing data. These models

primarily operate under a supervised training paradigm. This presents a fundamental application paradox: their training requires real, high-resolution time series, which are inherently lacking in the target application scenarios requiring interpolation. Furthermore, when the input time series lacks sufficient data points, these models will suffer significant performance decline because of inadequate contextual information [5].

To address this critical research gap, the present paper proposes a novel self-supervised time series SR method that combines Transformer (TF) and Generative Adversarial Network (GAN). First, the TF is introduced to address the insufficient contextual information issue. TF's attention mechanism and encoder-decoder architecture enable it to capture the global dynamics of the sequence. Second, the adversarial training framework of GAN ensures high fidelity in the dynamic properties and statistical distribution of the generated sequences. Third, through the computation of a feature space loss, the model generates high-resolution sequences that are consistent with the low-resolution input in terms of feature structure, without requiring actual high-resolution data. This self-supervised learning paradigm resolves the previously mentioned application paradox.

The main contributions of the present paper include:

- **Novel Method**: We propose a novel self-supervised time series interpolation training framework that operates without the need for real high-resolution data, thereby overcoming a major barrier for existing deep learning models.
- **Real Application**: We demonstrate the structure preserving properties of our method in model predictive control (MPC) applications, highlighting its potential for real-world energy systems.

The subsequent sections of this paper are organized as follows. Section 2 outlines our methods. Section 3 describes the experimental setup and data analysis. Section 4 provides with a discussion. Section 5 presents a review of related work, and Section 6 concludes a conclusion and an outlook.

2 Methodology

To address the limitations identified of Section 5, this paper presents an adaptive TF-GAN hybrid architecture for time series SR. The training process is mainly divided into three phases:

1. **Phase 1** is mainly used for pre-training the generator.
2. **Phase 2** is mainly used for pre-training the feature space discriminator.
3. **Phase 3** is mainly used for joint-training of the generator and discriminator.

The main design attributes will be introduced in the following sections individually.

2.1 Generator

A critical step in building a generative model for time series SR is selecting a suitable core generator architecture. Real-world data often exhibits significant variability. It may show different sample resolutions, contain missing values, and display periodic or seasonal trends. An effective model requires adaptability to deal with these features. Therefore, in the present paper, TF is used as the base model for the generator with its powerful sequence modeling capabilities and flexible architecture design. For details on the reasons for choosing TF as the base model, see Appendix A.

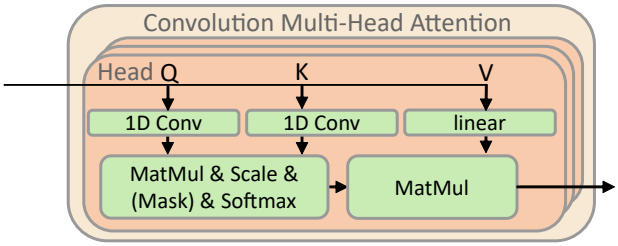

Figure 1: Modified attention mechanism used in the convolutional multi-head attention module.

Transformers utilize a self-attention mechanism that enables a model to process sequence elements in parallel and learn global dependencies [6]. The mechanism generates three vectors based on the input sequence: query (**Q**), key (**K**), and value (**V**) matrices, where queries and keys determine attention weights while values carry the actual information to be

aggregated. **Q** and **K** must have the same dimension, but **v** can have a different dimension, allowing it to map the input information into an output of a different dimension (or "length"), which is exactly what is needed for time series SR tasks (generating a high-resolution sequence from a low-resolution one). In the present paper, the task is to change the temporal resolution. Data points must be added, removed, or converted from the original dataset. Therefore, the short-term trend of the data points is of interest. Increasing the trend attention helps the data points recognize short-term patterns and better insert new points or delete old points. To address this need, a convolutional multi-head attention module [7] is employed, as illustrated at the top of Fig. 1. This module explicitly models trend changes in the data by capturing local contextual information for each data point. It ensures that each data point is aware of its context. The module uses 1D convolutional layers to extract these local trends, enhancing the model's understanding of short-term patterns.

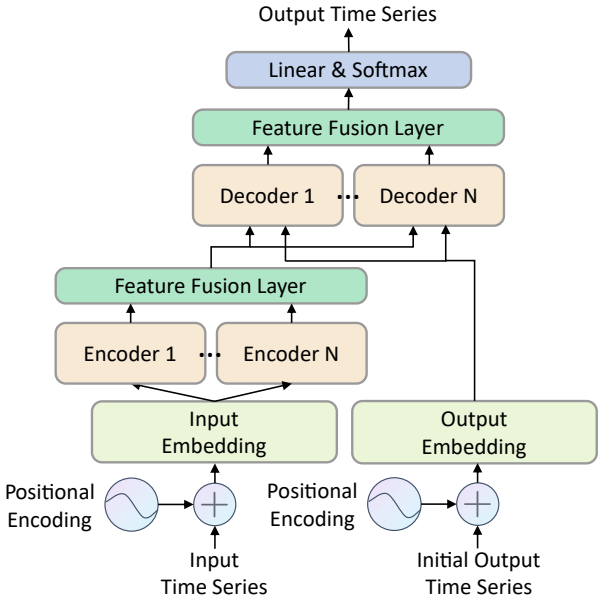

Figure 2: Generator of the modified GAN, consisting of encoder–decoder layers with feature fusion.

The outputs of the two attention mechanisms are combined in a feature fusion layer, resulting in a final feature matrix. A detailed description of this feature fusion layer (Multi-Scale Attention Aggregation [8]) can be found in Appendix B.

It is essential to note that due to the task of SR involved in the present work, all data point transformations are performed in the known time domain. Therefore, the causal masked multi-head attention mechanism will not be used.

In summary, the generator G used in the present paper is demonstrated in Fig. 2. It receives the following input:

- Input time series $X_{\text{input}} \in \mathbb{R}^{T_{\text{input}}}$ with the length of input time series T_{input}.
- Initial output time series $X_{\text{init}} \in \mathbb{R}^{T_{\text{output}}}$ with the length of output time series T_{output}. The initial time series is obtained by linear interpolation.

X_{input} is first embedded and then passed through the convolution encoder and the Fast Fourier Transform (FFT) encoder. After processing, the corresponding feature matrices are obtained. These feature matrices are fed into a feature fusion layer to produce the encoder's output. The encoder's output, along with X_{init}, is then provided to the decoder to generate the final output time series X_{output}. Using the above Transformer structure, it is possible to realize a generator G that supports input and output at arbitrary temporal resolution.

As our goal is neither predictive (autoregressive) nor sequence classification, conventional error measures as objectives such as Root Mean Squared Error (RMSE) or Mean Absolute Error (MAE) are unsuitable for the generator. This is especially true in our multi-resolution context, where the input x_{input} and the produced output $\hat{x}$ vary in both length and temporal granularity. The differences preclude direct point-wise comparison and require a loss design that is resilient to temporal misalignment and semantic variance. To address these issues, a combined loss function is implemented. It combines various loss functions to direct training. The primary design objective is to maintain both local numerical precision and global structural integrity while ensuring adaptability across various input resolutions. The total loss is a

weighted sum of all loss functions:

$$\mathcal{L}_{\text{total}} = \sum_i \lambda_i \mathcal{L}_i \tag{1}$$

Learnable weights [9] λ_i via a softPlus transformation are implemented to ensure the stability of the training process:

$$\lambda_i = \log\left(1 + e^{\alpha_i}\right), \quad \alpha_i \in \mathbb{R} \tag{2}$$

where α_i is the learnable parameter updated by backpropagation and the optimizer. These weights are trained jointly with the generator, enabling the model to emphasize the most informative supervision signals during learning dynamically. All loss functions used in the generator training process are listed in Appendix C. All initial weights are 1.

2.2 Discriminator

Although the combined loss function can improve the fit in terms of statistical features, it does not improve the fit when training the generator without the actual target data. However, such loss functions typically promote conservative forecasts and eventually converge to the mean. Furthermore, it is both impractical and futile to exhaust all the indicators. Simultaneously, conflicts may arise among several indicators, resulting in unreasonable training. By introducing the discriminator in the GAN, the model is able to learn implicit features of data. These features are difficult to encode through deterministic indicators [10, 11, 12]. The discriminator attempts to distinguish between authentic data from reality and synthetic data produced by the generator by learning the characteristics and distribution of the real data. In an ideal adversarial training process, the generator and the discriminator are trained together. Ultimately, the generator is capable of producing data that is indistinguishable from real data.

However, when dealing with tasks involving data of different lengths, such as resampling, a simple discriminator can easily distinguish between real data and generated data by only learning superficial representations such as sequence length, instead of learning the complex dynamic patterns within the sequence. Thus, the generator is not able to receive meaningful feedback, which hinders its learning ability. Furthermore, a standard mode collapse [13] problem arises in GAN training. That is, the structure of the discriminator may be too robust, causing its loss to converge to zero quickly. This results in the generator failing to receive an effective gradient signal, causing the training process to stagnate completely.

To address both challenges simultaneously, real and synthetic data will be distinguished in feature space, and a feature matching mechanism [13] will be introduced, as shown in Fig. 3. The core idea of this method is to adjust the optimization goal of the generator, which is no longer to maximize the classification error rate of the discriminator, but to make the features extracted from the generated data in the middle layer of the discriminator as similar as possible to the features of the real data. Specifically, the difference between the output of real and generated data in the discriminator's feature extraction layer is used as a new loss term to train the generator. Even if the discriminator has become very powerful and can perfectly distinguish between real and fake data, the generator can continue to learn and optimize by minimizing the feature differences between real and generated data. At the same time, the feature matching mechanism requires the generator to make the features of the generated data in the middle layer of the discriminator consistent with the real samples, thereby indirectly guiding the discriminator to focus on deeper feature expressions rather than simple surface features. So the feature space loss $\mathcal{L}_{\text{FM}}$ is introduced:

$$\begin{aligned}\mathcal{L}_{\text{FM}} = &||\mu(F_{X_{\text{input}}}) - \mu(F_{X_{\text{output}}})||_2^2 \\ &+ ||\sigma(F_{X_{\text{input}}}) - \sigma(F_{X_{\text{output}}})||_2^2\end{aligned} \tag{3}$$

It aims to minimize the difference in the mean (μ) and standard deviation (σ) of the feature representations of the input data and the output data in the intermediate layer of the discriminator.

2.3 Training Architecture

The whole training process is mainly divided into three phases, including pre- and joint-training processes. In the first phase, the generator focuses on pre-training. The generator is responsible for capturing the complex patterns and long-distance temporal dependencies of the time series. It receives the input data X_{input} and pre-processed initial X_{initial}, and is trained using the combined loss $\mathcal{L}_{\text{total}}$ to generate a high-resolution output time series.

The second phase aims to jointly train the feature space discriminator to obtain a usable feature space for the third phase. In this phase, the discriminator is jointly trained on the input data X_{input} and the output data X_{output} to learn how to distinguish between them effectively. At the same time, the generator is also trained with $\mathcal{L}_{\text{total}}$ and $\mathcal{L}_{\text{FM}}$ to ensure

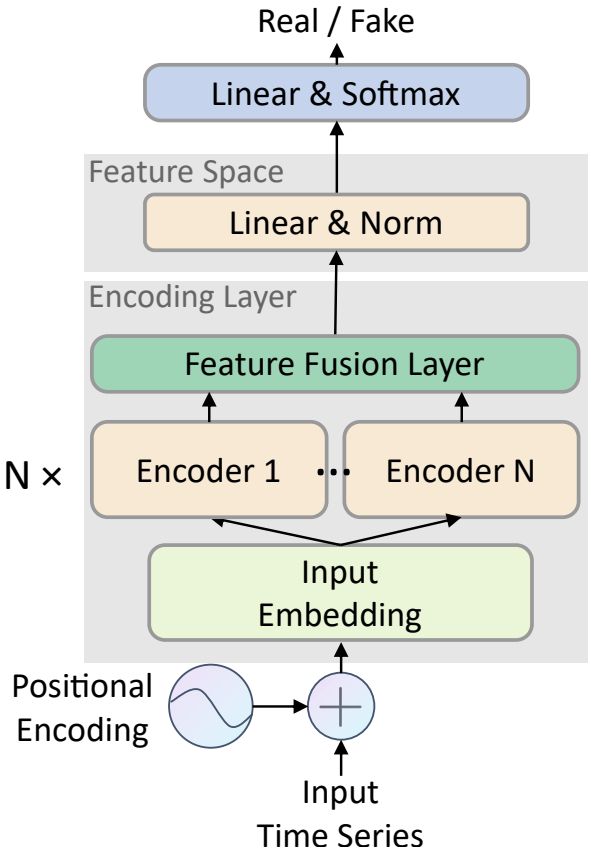

Figure 3: Discriminator of the modified GAN, consisting of Feature Space layers.

that the output data X_{output} matches the input data X_{input} in the feature space. The loss function of the discriminator in this phase uses Binary Cross-Entropy Loss (BCELoss) [14].

$$\begin{aligned}\mathcal{L}_{\text{D}} = & -\mathbb{E}_{X_{\text{input}}\sim p_{\text{data}}}\left[\log D(X_{\text{input}})\right] \\ & -\mathbb{E}_{X_{\text{output}}\sim p_g}\left[\log(1-D(X_{\text{output}}))\right]\end{aligned} \tag{4}$$

In the third phase, the trained discriminator is used as a feature space extractor. The generator continues to be trained separately using the extracted high-dimensional features. The core goal of the third phase is to learn how to generate time series data that is sufficient to deceive the discriminator. The output data X_{output} will match closely with the input data X_{input} in the feature space, ultimately achieving better time series upsampling.

3 Results

This section presents the experimental results of the present paper. First, the data set used will be introduced, followed by a performance evaluation of the model and an analysis of the results. Then, an application scenario is introduced. All single training results in the present paper were completed on a computer equipped with a 4070ti super GPU and a 7800x3d CPU.

3.1 Dataset

The WPuQ [15] dataset records the electric load data of 38 households in a small village in Lower Saxony, Germany. The present paper utilizes the indices NO_PV/SFH10/HOUSEHOLD for the 235-day power data P1.

PV-Live [16] is Europe's leading minute-level solar irradiance dataset, providing high-resolution measurements over the state of Baden-Württemberg, Germany. The dataset has been maintained collaboratively since September 2020,

encompassing data from 40 measurement stations with a one-minute resolution. The present paper utilizes the 363-day Solar Radiation (Gg_pyr) data from the 10th station in 2023 for the experiment.

The Wind Power dataset [17] contains data from 1 second to every hour, compared to the typical 10-minute interval for European wind power data. The present paper utilizes the entire dataset (81 days) for the experiment.

The mini-photovoltaic (MPV) benchmark dataset, known as MPVBench [18] contains real-time measurement data from five MPV, also known as balcony power plants in the Karlsruhe and Pforzheim regions. The present paper utilizes the entire 364-day solar power data from location 1a.

All data are resampled to 15-minute and 5-minute intervals, spanning 1 day, to verify the model's performance at varying intervals.

3.2 Ablation Experiment

Table 1: Performance Comparison - RMSE and PCC Metrics (lower RMSE and higher PCC indicate better performance) on the WPuQ [15], PV-Live [16], Wind Power [17], MPVBench [18] data sets

Metric	Phase	Method	WPuQ		PV-Live		Wind Power		MPVBench	
			Train	Test	Train	Test	Train	Test	Train	Test
RMSE	Phase 1	CONV	*0.3880*	*0.3758*	0.1994	0.2012	0.1821	0.1921	*0.1177*	*0.1180*
		SELF	0.4209	0.4148	0.3475	0.3435	0.3377	0.3408	0.2853	0.2912
		S+C	0.3958	0.3818	*0.1523*	*0.1538*	0.1878	0.1949	0.1304	0.1326
		S_C	0.3928	0.3795	0.2046	0.2010	*0.1818*	*0.1911*	0.1397	0.1394
	Phase 2	CONV	0.3383	0.3356	0.1059	0.1062	0.1536	0.1695	*0.0833*	*0.0830*
		SELF	0.4197	0.4204	0.3403	0.3356	0.3319	0.3325	0.2815	0.2870
		S+C	0.3402	0.3341	*0.1042*	*0.1042*	*0.1476*	0.1690	0.0847	0.0844
		S_C	*0.3261*	*0.3247*	0.1043	0.1044	0.1505	*0.1682*	0.0834	0.0841
	Phase 3	CONV	0.3453	0.3498	0.1032	0.1026	0.1487	0.1710	0.0797	0.0815
		SELF	0.4283	0.4255	0.3445	0.3393	0.3300	0.3337	0.2862	0.2915
		S+C	0.3459	0.3431	0.1020	0.1016	0.1477	0.1720	0.0821	0.0832
		S_C	**0.2983**	**0.3014**	**0.1011**	**0.0998**	**0.1407**	**0.1673**	**0.0782**	**0.0809**
	Static	Gauss	0.4056	0.4028	*0.1052*	*0.1059*	*0.1533*	*0.1665*	*0.0852*	*0.0846*
		Linear	*0.3816*	*0.3690*	0.1053	0.1060	0.1543	0.1676	0.0853	0.0847
		CSDI	0.6291	0.6243	0.1748	0.1765	0.3901	0.4036	0.1455	0.1533
PCC	Phase 1	CONV	0.7894	0.7980	0.9415	0.9387	*0.9578*	*0.9488*	*0.9726*	*0.9736*
		SELF	0.7388	0.7414	0.8031	0.8024	0.8445	0.8258	0.8144	0.8125
		S+C	0.7846	0.7941	*0.9655*	*0.9641*	0.9549	0.9463	0.9667	0.9671
		S_C	*0.7895*	*0.7985*	0.9358	0.9360	0.9566	0.9477	0.9582	0.9596
	Phase 2	CONV	0.8405	0.8400	0.9832	0.9826	0.9691	0.9591	0.9853	*0.9859*
		SELF	0.7378	0.7316	0.8077	0.8080	0.8472	0.8321	0.8172	0.8156
		S+C	0.8389	0.8418	*0.9836*	*0.9832*	*0.9715*	0.9592	0.9849	0.9855
		S_C	*0.8528*	*0.8513*	0.9835	0.9831	0.9710	**0.9600**	*0.9854*	0.9856
	Phase 3	CONV	0.8384	0.8308	0.9839	0.9836	0.9715	0.9587	0.9866	0.9865
		SELF	0.7292	0.7262	0.8027	0.8038	0.8487	0.8301	0.8106	0.8095
		S+C	0.8364	0.8357	0.9843	0.9840	0.9720	0.9583	0.9858	0.9858
		S_C	**0.8775**	**0.8723**	**0.9846**	**0.9846**	**0.9741**	*0.9599*	**0.9871**	**0.9866**
	Static	Gauss	0.7579	0.7571	*0.9833*	*0.9827*	*0.9692*	*0.9603*	*0.9847*	*0.9854*
		Linear	*0.7939*	*0.8033*	0.9832	0.9826	0.9689	0.9599	0.9846	0.9853
		CSDI	0.4926	0.4836	0.9541	0.9519	0.8049	0.7645	0.9554	0.9511

First, an ablation experiment is conducted on the training architecture and attention mechanism structure introduced in this paper. Tab. 1 summarizes the performance at different training stages (Phases) and different methods (Methods) for different datasets (WPuQ [15], PV-Live [16], Wind Power [17], MPVBench [18]). Italic and underlined numbers indicate the best performance within a single phase, while bold green numbers indicate the best performance across all phases. The evaluation indicators include the root mean square error (RMSE) and the Pearson Correlation Coefficient (PCC). The results for each dataset are presented separately for the training set (Train) and the test set (Test). Additionally, Static refers to the linear interpolation, Gauss Process and Conditional Score-based Diffusion models for Imputation (CSDI) [19] used as a performance benchmark. In order to adapt to the time series upsampling task, the mask used by CSDI will be fixed. That is, a high-resolution signal is recovered from a fixed, sparse low-resolution signal.

The attention mechanisms used in our method include:

- SELF, which refers to the traditional Transformer self-attention mechanism,

- CONV, the convolutional attention mechanism used in this paper,
- S+C, the serial combination of the self-attention layer and the convolutional attention layer, and
- S_C, the parallel connection of the self-attention mechanism and the convolutional attention mechanism through the feature fusion layer.

The best model in each stage is saved independently based on the loss performance of the test set during training. The training of the subsequent stage is based on the best model of the previous stage, but the best test set loss from the previous model will not be recorded. The values shown in Tab. 1 are the comparison between the output data X_{output} and the real data X_{real}. It should be emphasized that the real data X_{real} has never been used in training. Only the input data X_{input} is used to calculate the training loss during the entire training process.

The performance of current benchmark models is first evaluated. In Tab. 1, phase "Static" shows that the RMSE is significantly lower for both Gaussian processes and linear interpolation than for the CSDI method. There is only a little difference in performance between the Gaussian process and linear interpolation. This reveals another contextual limitation of interpolation models, which is described shortly in Section 5. In time series upsampling tasks, the target high-resolution sequence is often several times longer than the low-resolution sequence. This leads to a very sparse mask matrix of known points and can dramatically increase the uncertainty of the imputation model, ultimately leading to suboptimal upsampling results.

After analyzing the performance of existing baseline models, the contributions of the introduced method and its key components will now be evaluated. From Tab. 1, Phase 2 and Phase 3 generally have a better model performance than Phase 1 on all datasets, performance indicators (RMSE, PCC), and training and test sets. This result clearly indicates that introducing the discriminator structure can significantly improve the model's training quality. Taking the RMSE on the test set of the WPuQ dataset as an example, the RMSE of S+C in Phase 1 is 0.3818, while the RMSE of S+C in Phase 2 is reduced to 0.3341, a decrease of about $12.49\ \%$. For the PV-Live test set, the RMSE of CONV in Phase 1 is 0.2012, while the RMSE in Phase 2 is reduced to 0.1062, a decrease of about $47.22\ \%$. In contrast, the model using only the SELF method yielded relatively poor results in all indicators across all training stages and nearly all datasets. This indicates that for such SR tasks, the self-attention mechanism alone is insufficient to capture and utilize the key information in the data effectively. This proves that the introduction of convolutional attention is practical. For example, on the wind test set, the RMSE of SELF in Phase 1 is 0.3408, while S+C is 0.1949, and SELF is about $42.81\ \%$ higher.

The S_C method usually achieves lower RMSE and higher PCC, indicating that the parallel structure is more suitable for accurately fitting the training data. The numbers marked in red in the table show that the S_C structure of Phase 3 achieves the best results on all datasets. It is only inferior to the S_C structure of Phase 2 on the wind test set, but the gap is less than $0.01\ \%$. Compared with the static interpolation method used as a benchmark, the S_C structure has an average performance lead of $9\ \%$ in RMSE. In PCC, this value is $2.5\ \%$.

To verify the validity of the above conclusions, a significance test was performed. The detailed results of the significance test can be found in Appendix D. Judging by the results of the significance test, the S_C has a significant advantage in Phase 3 compared with the Gauss Process and SELF structures. However, compared to CONV and S+C, in Phase 3 S_C has a slight advantage in fitting the training set, but it is not significant in the test set.

3.3 MPC Application Scenario

Modern energy systems incorporating renewable energy, energy storage, and smart grids are highly dynamic. The operation of these networks is influenced by various factors, including weather fluctuations, user behavior, and intermittent renewable energy production, leading to ongoing changes in their state and load. Co-simulation provides a practical framework. It allows for the integration of multiple specialized models from different domains and timescales to simulate the dynamic behavior of the entire system. Models that integrate Model Predictive Control (MPC) are frequently used in co-simulation, such as MPC models for controlling energy storage systems. MPC optimizes the future operation of the system by calculating the optimal trajectory of the system's control output, while considering the system's future behavior [20]. In each control period, MPC uses the current system state, the predicted future data, and the system model to solve an optimization problem within a limited time window (Prediction Horizon) to obtain the optimal control strategy. Then, MPC only executes the first control action in the strategy and repeats the whole process for the next sampling period. The performance of MPC depends heavily on both model accuracy and data accuracy. High resolution, such as 1-minute data, helps to learn and predict the dynamic behavior of energy systems more accurately, thereby improving the control accuracy and energy-saving effect of MPC. For example, Chen et al. [21] used 10-second data for MPC based on data-driven learning to deal with high-energy consumption systems, effectively predict system dynamics, and efficiently control various devices, thereby reducing energy consumption. Additionally, with the increasing penetration of renewable energy sources (such as solar and wind energy), grid management has become more complex. High resolution can better understand the real impact of these energy sources and make better

operational decisions [22]. In contrast, low resolution, such as 1-hour data, requires relatively little computing power. It may miss short-term fluctuations and lack sensitivity for real-time control [23].

Therefore, if high-resolution MPC is required, such as for refined scheduling or real-time optimization, high-resolution time series data is required. However, in practical applications, the availability of high-resolution data may not be met. The data may have only low resolution due to sensor limitations, insufficient acquisition frequency, or storage costs. Additionally, the data may originate from the output of other models, and the output resolution of these models does not meet the requirements of MPC. In these cases, to meet the requirements of high-resolution MPC, it is necessary to upsample the existing data.

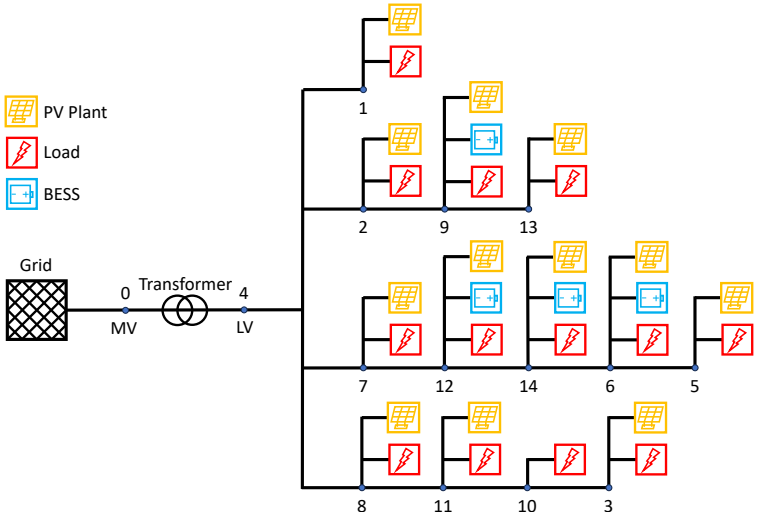

Figure 4: The electrical grid based on [24] and [25] was used as an application scenario.

In the present paper, a scenario from [25], as shown in Fig. 4, is used. It uses the benchmark network "1-LV-rural1-1-sw" from simbench [24], and on this basis, four solar generation plants are added to the original grid at nodes 6, 9, 12, and 14, which are equipped with battery storage. These battery storages are controlled using the MPC described in [25]. The network data has a resolution of 15 minutes, which will be downsampled to 1 hour. Then it will be upsampled again to a 15-minute time series using the method S_C and S+C with Phase 3 described in the present paper.

Table 2: Performance Comparison of Electrical Grid - RMSE and PCC Metrics (lower RMSE and higher PCC indicate better performance)

		L1-A				**L2-A**				**Soil_Alternative_2**				**PV5**	
		P		Q		P		Q		P		Q		pv	
		Train	Test	Train	Test	Train	Test	Train	Test	Train	Test	Train	Test	Train	Test
PCC	Gauss	0.8908	0.8722	0.9274	**0.8850**	0.8987	**0.9041**	0.8785	**0.8817**	0.8930	0.8758	0.8930	0.8758	0.9974	0.9961
	S+C	0.9331	**0.8730**	0.9501	0.8791	0.9434	0.9030	0.9202	0.8734	0.9029	0.8855	0.9029	0.8855	**0.9981**	**0.9968**
	S_C	**0.9504**	0.8692	**0.9706**	0.8763	**0.9567**	0.9023	**0.9487**	0.8678	**0.9100**	**0.8939**	**0.9083**	**0.8927**	0.9975	0.9962
RMSE	Gauss	0.2195	0.2360	0.1864	**0.2320**	0.2175	**0.2147**	0.2322	**0.2297**	0.3117	0.3470	0.3117	0.3470	0.0496	0.0568
	S+C	0.1727	**0.2353**	0.1559	0.2383	0.1652	0.2177	0.1917	0.2405	0.2976	0.3337	0.2976	0.3337	0.0469	0.0544
	S_C	**0.1508**	0.2382	**0.1208**	0.2404	**0.1488**	0.2160	**0.1558**	0.2410	**0.2875**	**0.3227**	**0.2900**	**0.3245**	**0.0328**	**0.0451**
		H0-A				**H0-B**				**H0-C**				**PV6**	
		P		Q		P		Q		P		Q		pv	
		Train	Test	Train	Test	Train	Test	Train	Test	Train	Test	Train	Test	Train	Test
PCC	Gauss	0.8402	**0.8502**	0.5982	0.5911	0.7668	**0.7339**	0.6136	0.6447	0.8145	**0.8567**	0.5856	0.6098	0.9974	0.9961
	S+C	0.9032	0.8425	0.7859	0.6176	0.8735	0.7325	0.7623	**0.6791**	0.8984	0.8427	0.7763	**0.6425**	**0.9986**	**0.9965**
	S_C	**0.9270**	0.8340	**0.8368**	**0.6184**	**0.9115**	0.7262	**0.7965**	0.6734	**0.9316**	0.8361	**0.8238**	0.6425	0.9975	0.9958
RMSE	Gauss	0.2505	**0.2508**	0.3285	0.3010	0.2577	0.2805	0.3179	0.3113	0.2486	**0.2280**	0.3342	0.2999	0.0494	0.0558
	S+C	0.1961	0.2556	0.2393	**0.3010**	0.1928	**0.2759**	0.2476	**0.2839**	0.1882	0.2389	0.2455	**0.2999**	**0.0355**	**0.0523**
	S_C	**0.1735**	0.2602	**0.2125**	0.3011	**0.1644**	0.2788	**0.2314**	0.2866	**0.1585**	0.2442	**0.2215**	0.3065	0.0485	0.0550

In this Section, if the test loss of Phase 3 does not continue to decrease compared to Phase 2, then early stopping will be performed. Tab. 2 shows the results of SR. The best results for each dataset is indicated in bold. From the results in the table, the error of S_C on the most training sets including active power P and inactive power Q is significantly lower than that of S+C and Gauss Process. It is consistent with its ability to fit the training set mentioned above. It is worth reiterating that no high-resolution time series is involved in the training process. However, the fitting performance and generalization performance of S_C on the photovoltaic dataset are not superior to those of S+C. The RMSE values

for the PV dataset PV6 are generally much lower than those for the other datasets, which may suggest its inherent smoothness or higher predictability. However, some numerical fluctuations will cause relatively large errors.

Table 3: Results of MPC - RMSE and MAE Metrics (lower RMSE and higher PCC indicate better performance)

	RMSE [kW]	MAE [kW]
Gauss	3.0142	1.376
S+C	2.910	1.21
S_C	2.651	1.184

In the presented application scenario, data sampled by different methods are imported into the MPC model. The power curves of the four batteries are calculated. The curves obtained are then compared with the results simulated with real high-resolution data. This is used to evaluate the control error caused by the SR error. Tab. 3 shows the results of MPC simulation. Method S_C maintains its leading position this time. Compared with Gauss Process, S_C has an improvement of $12.05\ \%$ in RMSE and $13.95\ \%$ in MAE.

4 Discussion

This paper introduces an effective solution to the time resolution mismatch challenge faced by complex energy network coupling modeling in the context of energy system decarbonization. The core design of this method features an adaptive encoder-decoder framework based on the Transformer, capable of handling time series of variable length and resolution. An improved attention mechanism that specifically combines convolutional multi-head attention for local trend extraction and traditional self-attention for global dependencies, integrated through a multi-scale attention aggregation mechanism. A three-phase self-supervised training strategy: Stage 1 focuses on generator pre-training using combined loss functions; Stage 2 introduces joint adversarial training between generator and discriminator; Stage 3 emphasizes feature space optimization through a feature matching mechanism. This method has advanced in preserving data fidelity. The strategy presented in this paper, particularly with the use of the GAN discriminator, enhances the preservation of statistical and temporal validity of the data during the resolution conversion process. It again must be emphasized that the training method solely relies on existing low-resolution data, without incorporating any high-resolution data. This is more in line with the needs of actual tasks.

The proposed method demonstrates good performance on multiple real-world energy datasets, including photovoltaic (PV-Live, MPV), wind power (Wind Power), and load (WPUQ). Experimental results demonstrate its superiority over conventional upsampling methods. Experimental results show that this method outperforms traditional methods in SR tasks of real energy datasets such as PV-Live, Wind Power, WPUQ, and MPV. For example, it leads by an average of 9 % in RMSE and 2.5 % in Pearson Correlation Coefficient (PCC). The significance test show the improvement effect of layering: First, the introduction of the discriminator (Phase 2 vs. Phase 1) brings statistically significant performance improvement. Second, the convolutional attention mechanism has a considerable advantage over pure self-attention (CONV vs. SELF). However, the differences between different attention fusion strategies (CONV, S+C, S_C) are relatively small and not always statistically significant. Although the different variants proposed in this study have numerical differences, the statistical significance test reveals a critical finding: after the core improvements obtained through the discriminator and convolutional attention, the marginal benefits brought by further optimization of architectural details are limited.

In addition, the effectiveness and practical value of this method are verified by applying it to the control of battery energy storage systems in the model predictive control (MPC) power grid scenario. Compared to traditional methods, the results obtained using the method presented in this paper are more closely aligned with simulation results based on real data. It provides a data-driven solution for time resolution matching in energy network modeling.

Limitations of this study include that the evaluation focused on the conversion from 15-min to 5-min resolution and from 1-h to 15-min, and that the performance improvements varied for different types of energy data (e.g., PV data showed lower improvements than load data).

5 Related Work

Data intertransformation is an unavoidable problem in the interaction between different models during the co-simulation. As mentioned in Sec. 1, efficiently and accurately transforming time-series data is essential for achieving accurate model coupling and minimizing errors caused by temporal mismatches. To address the temporal mismatch issue, researchers frequently employ resampling techniques. These include upsampling for filling in low-resolution data [26] and downsampling for condensing high-resolution data [27]. Compared with downsampling, upsampling of data is more

prone to introducing errors. Upsampling necessitates the creation of new data points via interpolation or alternative estimation techniques. Interpolation is a widely used time series resolution upsampling method, but its applicability is limited to the specific characteristics of the dataset [28]. For instance, Omoyele et al. [22] evaluated time series upsampling methods in energy systems. Their study focused on two key data categories: solar and wind. For solar data, the non-dimensional technique offers better results. For wind data, a mix of physical models and stochastic fluctuations is more successful.

Lepot et al. [26] reviewed a variety of interpolation methods and pointed out that most interpolation methods lack an evaluation framework separate from specific algorithms, making it difficult to establish universal performance benchmarks. Additionally, each upsampling method is based on specific assumptions about the data's characteristics. When the data does not align with these assumptions, the quality of the generated data is significantly compromised.

To address the limitations of traditional upsampling methods, researchers have increasingly turned to advanced machine learning techniques, such as time series generation, SR and imputation models. Traditional time series generation models focus on learning and reconstructing the underlying distributions of original data to generate new high-resolution sequences with similar statistical properties. The concept of SR originates from computer vision, aiming to establish an accurate mapping from a low-resolution sequence to a high-resolution sequence. Time series imputation is a broader concept that refers to various techniques for filling in missing data points.

Super-Resolution (SR) is a crucial technique for enhancing data resolution. SR combines upsampling with deep neural networks to recover more details by learning from low- and high-resolution data. SR not only increases the sampling rate of the time series, but also uses methods such as deep learning to recover or reconstruct the lost details and high-frequency information in the time series. It is making the result closer to the real high-sampling time series. It is widely used in image processing [29], point cloud reconstruction [30], and other fields. However, compared to the popularity of SR in the field of images and point clouds, there are relatively few studies on SR in the field of time series. Han and Wang [31] are the first researchers to apply the combination of Recurrent Neural Network (RNN) and GAN to generate high-resolution temporal volume sequences. However, the training process requires the use of real high-resolution data to calculate the loss. In practical situations, this presents a paradox: if the high-resolution data already exists, why is there a necessity to interpolate it from low-resolution data?

This data availability challenge also exists in the field of time series imputation, which shares similar methodological foundations with the upsampling task. Time series imputation focuses on filling missing values in a series, which can also be considered a special case of upsampling. Important research in this area includes GRU-D [32], which modifies the Gated Recurrent Unit (GRU) to incorporate missing pattern information, BRITS [33], which leverages bidirectional recurrent dynamic systems to learn imputation, and CSDI [19], which learns to reverse a diffusion process to reconstruct missing data points. These models are typically trained in a self-supervised paradigm, where values are artificially masked from the full real dataset and the model's task is to reconstruct these masked values accurately. Thus, similar to the challenges in time series SR, the training process of these imputation models also presupposes the availability of complete data, which contradicts the unavailability of high-resolution data in upsampling tasks. Moreover, in upsampling tasks, known points are typically sparse, resulting in the model having limited reference data points during input, which can easily lead to insufficient contextual information and suboptimal outcomes [5].

Although the goals of traditional generative models and upsampling tasks are inconsistent, advanced generative models (such as generative adversarial networks (GANs) or diffusion models) can achieve upsampling through "conditional generation" [34]. GANs are artificial intelligence methods used to solve the sample generation problem [35]. Its goal is to study a set of training samples, learn the probability distribution that generates those samples, and generate additional samples based on this probability distribution. Tang et al. [36] interpolated solar data using GANs, marking the first use to generate time series with different resolutions [22]. Moreover, its limitation is that the model structure is bound to a specific resolution and length. The model structure is hardcoded for specific use cases. It works only with two fixed temporal resolutions and lengths, such as a 30-minute input and a 5-minute output resolution. However, most research [10, 37] on time series GAN focuses on data enhancement, i.e., techniques aimed at improving the quality of existing datasets through synthetic data generation. The MC-TimeGAN introduced by Demirel et al. [38] can generate multivariate synthetic time series conditioned on labels, focusing on synthetic grid congestion scenarios. Their work mentioned the possibility of generating time series with varying resolutions. However, the core goal of their research is to generate event-specific conditional data, not a generalized resolution conversion tool. Therefore, although GANs have great potential in ensuring high fidelity of generated data, existing work has not yet provided a mature framework that can adapt to arbitrary resolutions and is designed explicitly for unsupervised upsampling tasks.

In addition to the pursuit of high fidelity, it is also crucial to address the issue of insufficient contextual information caused by sparse input points. In this regard, the Transformer (TF) architecture demonstrates significant advantages thanks to its attention mechanism. This mechanism captures long-term time dependencies and complex multivariate correlations while enabling parallel processing [6]. These properties have been successful in several areas, including

time series prediction, classification, and anomaly detection [39]. However, relatively little work has focused on time series upsampling. Multi-scale attention [40] and frequency-domain attention [41] represent significant advancements in the TF architecture. The multi-scale attention mechanism offers significant advantages for resolution transformation. It enables the model to simultaneously capture local patterns and global trends at different temporal granularities. This capability is critical for maintaining or reconstructing information while transforming resolution [40]. The frequency-domain attention mechanism provides another advantage. It enables TFs to directly manipulate spectral components, offering a more principled method to resolution conversion. This method maintains significant frequency features [41]. The application of these mechanisms demonstrates the potential of TFs in resampling tasks, as they can adaptively focus on the most relevant temporal and spectral features to achieve accurate resolution conversion.

TFs focus on understanding dependencies between data points, while GANs demonstrate superior skill in creating high-quality synthetic data. Together, they provide a reasonable method for time series upsampling. In the coupling of energy network models, the input and output time series resolution is often not fixed, thereby the GANs structure has to be designed to be adaptive to different resolutions. Through the above analysis, existing research has shortcomings in the following aspects:

- **Context**: When the input data points are extremely sparse, the model lacks sufficient context for the task.
- **Fidelity**: Traditional upsampling methods may lose details and local features in the original data.
- **Data Dependency**: The requirement of the upsampling task itself is based on the fact that high-resolution data is missing. However, there is no method for training entirely based on low-resolution data.

6 Conclusion and Outlook

To address the data challenges caused by temporal granularity mismatch in energy system co-simulation, this paper proposes a self-supervised super-resolution framework based on a Generative Adversarial Transformer. This method not only overcomes the limitations of conventional interpolation methods but also overcomes a paradox of supervised learning in upsampling scenarios: supervised training requires a high-resolution time series that is absent in upsampling applications. Without requiring high-resolution data, this method reduces the RMSE by an average of 9% on multiple real-world energy datasets and improves the accuracy of a MPC application by 13%.

Future research will focus more on structural innovation, like compressing three phases into one, and larger-scale experiments are being investigated to verify the statistical reliability of these subtle improvements.

Acknowledgements

This work is supported in part by the Helmholtz Association through the project "Helmholtz Platform for the Design of Robust Energy Systems and Their Supply Chains" (RESUR), the Helmholtz Energy System Design (ESD) program, and the Helmholtz AI HAICORE partition (HAICORE@KIT).

References

[1] Elisa Papadis and George Tsatsaronis. Challenges in the decarbonization of the energy sector. *Energy*, 205: 118025, 2020. ISSN 0360-5442. doi: https://doi.org/10.1016/j.energy.2020.118025. URL `https://www.sciencedirect.com/science/article/pii/S0360544220311324`.

[2] Miguel Chang et al. Trends in tools and approaches for modelling the energy transition. *Applied Energy*, 290:116731, 2021. ISSN 0306-2619. doi: https://doi.org/10.1016/j.apenergy.2021.116731. URL `https://www.sciencedirect.com/science/article/pii/S0306261921002476`.

[3] Karl-Kiên Cao et al. Bridging granularity gaps to decarbonize large-scale energy systems—the case of power system planning. *Energy Science & Engineering*, 9(8):1052–1060, 2021. doi: https://doi.org/10.1002/ese3.891. URL `https://scijournals.onlinelibrary.wiley.com/doi/abs/10.1002/ese3.891`.

[4] Kris Poncelet et al. Impact of the level of temporal and operational detail in energy-system planning models. *Applied Energy*, 162:631–643, 2016. ISSN 0306-2619. doi: https://doi.org/10.1016/j.apenergy.2015.10.100. URL `https://www.sciencedirect.com/science/article/pii/S0306261915013276`.

[5] Georgios Batzolis, Jan Stanczuk, Carola-Bibiane Schönlieb, and Christian Etmann. Conditional image generation with score-based diffusion models. *arXiv preprint arXiv:2111.13606*, 2021.

[6] Yifan Xu et al. Transformers in computational visual media: A survey. *Computational Visual Media*, 8:33–62, 2022. doi: 10.1007/s41095-021-0247-3.

[7] Shengnan Guo et al. Learning dynamics and heterogeneity of spatial-temporal graph data for traffic forecasting. *IEEE Transactions on Knowledge and Data Engineering*, 34(11):5415–5428, 2022. doi: 10.1109/TKDE.2021.3056502.

[8] Mushui Liu, Jun Dan, Ziqian Lu, Yunlong Yu, Yingming Li, and Xi Li. Cm-unet: Hybrid cnn-mamba unet for remote sensing image semantic segmentation, 2024. URL https://arxiv.org/abs/2405.10530.

[9] Alex Kendall et al. Multi-task learning using uncertainty to weigh losses for scene geometry and semantics. In *Proceedings of the IEEE Conference on Computer Vision and Pattern Recognition*, pages 7482–7491, 2018.

[10] Jinsung Yoon et al. Time-series generative adversarial networks. In H. Wallach, H. Larochelle, A. Beygelzimer, F. d'Alché-Buc, E. Fox, and R. Garnett, editors, *Advances in Neural Information Processing Systems*, volume 32. Curran Associates, Inc., 2019.

[11] Xiaomin Li et al. Tts-gan: A transformer-based time-series generative adversarial network, 2022. URL https://arxiv.org/abs/2202.02691.

[12] Richard Zhang et al. The unreasonable effectiveness of deep features as a perceptual metric. In *Proceedings of the IEEE conference on computer vision and pattern recognition*, pages 586–595, 2018.

[13] Tim Salimans et al. Improved techniques for training gans. *Advances in neural information processing systems*, 29, 2016.

[14] Ian J. Goodfellow et al. Generative adversarial nets, 2014. URL https://arxiv.org/abs/1406.2661.

[15] Marlon Schlemminger et al. Dataset on electrical single-family house and heat pump load profiles in germany. *Scientific data*, 9(1):56, 2022.

[16] A Dittmann et al. Pv-live dataset-measurements of global horizontal and tilted solar irradiance, 2022.

[17] Daniel Vázquez Pombo et al. Multi-horizon data-driven wind power forecast: From nowcast to 2 days-ahead. In *2021 International Conference on Smart Energy Systems and Technologies (SEST)*, pages 1–6. IEEE, 2021.

[18] Gökhan Demirel et al. PIDE: Photovoltaic integration dynamics and efficiency for autonomous control on power distribution grids. *Energy Informatics*, 8(1):32, 2025. ISSN 2520-8942.

[19] Yusuke Tashiro, Jiaming Song, Yang Song, and Stefano Ermon. Csdi: Conditional score-based diffusion models for probabilistic time series imputation. *Advances in neural information processing systems*, 34:24804–24816, 2021.

[20] Diego I. Hidalgo-Rodríguez and Johanna Myrzik. Optimal operation of interconnected home-microgrids with flexible thermal loads: A comparison of decentralized, centralized, and hierarchical-distributed model predictive control. In *2018 PSCC*, pages 1–7, 2018. doi: 10.23919/PSCC.2018.8442807.

[21] Jiawei Chen, Gangyan Xu, and Ziye Zhou. Data-driven learning-based model predictive control for energy-intensive systems. *Advanced Engineering Informatics*, 58:102208, 2023.

[22] Olalekan Omoyele et al. Increasing the resolution of solar and wind time series for energy system modeling: A review. *Renewable and Sustainable Energy Reviews*, 189:113792, 2024. ISSN 1364-0321. doi: https://doi.org/10.1016/j.rser.2023.113792. URL https://www.sciencedirect.com/science/article/pii/S1364032123006494.

[23] Stefan Pfenninger. Dealing with multiple decades of hourly wind and pv time series in energy models: A comparison of methods to reduce time resolution and the planning implications of inter-annual variability. *Applied energy*, 197:1–13, 2017.

[24] Steffen Meinecke et al. Simbench—a benchmark dataset of electric power systems to compare innovative solutions based on power flow analysis. *Energies*, 13(12), 2020. ISSN 1996-1073.

[25] Felicitas Mueller et al. Sector-coupled distribution grid analysis for centralized and decentralized energy optimization. In *2023 58th International UPEC*, pages 1–6. IEEE, 2023.

[26] Mathieu Lepot et al. Interpolation in time series: An introductive overview of existing methods, their performance criteria and uncertainty assessment. *Water*, 9(10), 2017. ISSN 2073-4441. doi: 10.3390/w9100796. URL https://www.mdpi.com/2073-4441/9/10/796.

[27] Mahmoud Nassar et al. Aggregation techniques for time series data: A survey. *Journal of Big Data*, 7(1):1–18, 2020.

[28] Maximilian Hoffmann, Leander Kotzur, Detlef Stolten, and Martin Robinius. A review on time series aggregation methods for energy system models. *Energies*, 13(3), 2020. ISSN 1996-1073. doi: 10.3390/en13030641. URL https://www.mdpi.com/1996-1073/13/3/641.

[29] Zhiguo Cao et al. Learning to upsample by learning to sample. *2023 IEEE/CVF International Conference on Computer Vision (ICCV)*, pages 6004–6014, 2023. doi: 10.1109/ICCV51070.2023.00554.

[30] D. Cohen-Or et al. Pu-net: Point cloud upsampling network. *2018 IEEE/CVF Conference on Computer Vision and Pattern Recognition*, pages 2790–2799, 2018. doi: 10.1109/CVPR.2018.00295.

[31] Jun Han and Chaoli Wang. Tsr-tvd: Temporal super-resolution for time-varying data analysis and visualization. *IEEE Transactions on Visualization and Computer Graphics*, 26:205–215, 2020. doi: 10.1109/TVCG.2019.2934255.

[32] Zhengping Che, Sanjay Purushotham, Kyunghyun Cho, David Sontag, and Yan Liu. Recurrent neural networks for multivariate time series with missing values. *Scientific reports*, 8(1):6085, 2018.

[33] Wei Cao, Dong Wang, Jian Li, Hao Zhou, Lei Li, and Yitan Li. Brits: Bidirectional recurrent imputation for time series. *Advances in neural information processing systems*, 31, 2018.

[34] Eoin Brophy et al. Generative adversarial networks in time series: A systematic literature review. *ACM Comput. Surv.*, 55(10), February 2023. ISSN 0360-0300. doi: 10.1145/3559540. URL https://doi.org/10.1145/3559540.

[35] Ian Goodfellow et al. Generative adversarial networks. *Commun. ACM*, 63(11):139–144, October 2020. ISSN 0001-0782. doi: 10.1145/3422622. URL https://doi.org/10.1145/3422622.

[36] Rui Tang et al. Interpolating high granularity solar generation and load consumption data using super resolution generative adversarial network. *Applied Energy*, 299:117297, 2021. ISSN 0306-2619. doi: https://doi.org/10.1016/j.apenergy.2021.117297. URL https://www.sciencedirect.com/science/article/pii/S0306261921007108.

[37] Abdellah Madane et al. Transformer-based conditional generative adversarial network for multivariate time series generation, 2022. URL https://arxiv.org/abs/2210.02089.

[38] Gökhan Demirel et al. Synthesizing Distribution Grid Congestion Data Using Multivariate Conditional Time Series Generative Adversarial Networks. In *2024 IEEE iSPEC*, pages 385–390, 11 2024.

[39] Yuxuan Wang et al. Deep time series models: A comprehensive survey and benchmark. *arXiv preprint arXiv:2407.13278*, 2024.

[40] Shizhan Liu et al. Pyraformer: Low-complexity pyramidal attention for long-range time series modeling and forecasting. In *International Conference on Learning Representations*, 2022. doi: 10.34726/2945. URL https://openreview.net/forum?id=0EXmFzUn5I.

[41] Tian Zhou et al. Fedformer: Frequency enhanced decomposed transformer for long-term series forecasting. In *International conference on machine learning*, pages 27268–27286. PMLR, 2022.

[42] E. Hewitt and R. E. Hewitt. The gibbs-wilbraham phenomenon: An episode in fourier analysis. *Archive for History of Exact Sciences*, 21(2):129–160, 1979.

A Baseline Selection

This section employs Long Short-Term Memory (LSTM), Temporal Convolutional Network (TCN), and TF as baseline models, which exemplify three fundamental and significant methodologies in time series analysis [39]. LSTM, as a prototypical recurrent neural network (RNN), is a well-established architecture designed for sequence data processing and is widely used in time series research. TCN denotes the utilization of convolutional neural networks (CNN), which excel at identifying local features and patterns in data via convolutional operations. The TF, utilizing its robust self-attention mechanism, has exhibited exceptional proficiency in capturing long-term temporal dependencies and intricate connections, establishing itself as a sophisticated backbone architecture. To evaluate the performance of the candidate architectures presented above, a series of controlled experiments for interpolation on a variety of waveform tasks are introduced, including simple linear trends, square waves with mutations, smooth sinusoids, and sawtooth patterns exhibiting discontinuities. All networks use the most basic structure. Fig. 5 shows the results of three models in four types of waveform interpolation tasks. In the linear waveform task, whereas LSTM is closer to the real trend line, TF TCN has prominent oscillations. The square wave task best reflects the difference between the models. TF captures the jump transition. However, LSTM has a smoothing phenomenon at the transition point and cannot maintain sharp edges, and produces the Gibbs phenomenon [42]. TCN still maintains severe oscillations. In the triangle wave test, TF and LSTM can maintain the sharp peak characteristics well, but only exhibit a certain degree of smoothing effect, resulting in rounded peaks. TCN exhibits the most severe oscillation in all tasks. However, LSTM has a significant error at the beginning of the output due to limited context. That is, the model based on the RNN structure can only see

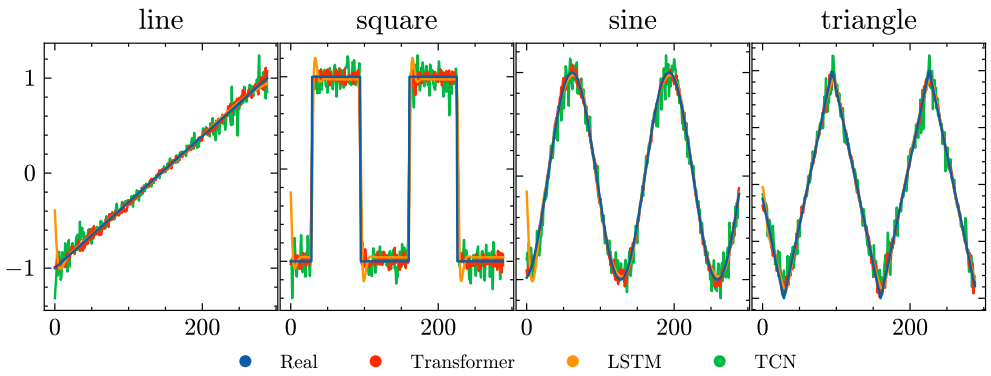

Figure 5: Baseline Selection.

information from the past. This causes the model to show significant deviations at key points of the resampled signal (such as the beginning or step of the sequence). Overall, TF has advantages in processing various complex waveforms, especially those containing discontinuities.

Table 4: Performance Metrics Comparison

Metric	Model	Line	Square	Sine	Triangle
RMSE	TCN	0.0758	0.2049	0.1012	0.0857
	LSTM	0.0491	0.2090	0.0599	0.0515
	TF	**0.0356**	**0.1721**	**0.0403**	**0.0359**
MAE	TCN	0.0528	0.1167	0.0761	0.0644
	LSTM	**0.0160**	0.0839	**0.0274**	**0.0255**
	TF	0.0272	**0.0659**	0.0311	0.0271
PCC	TCN	0.9914	0.9788	0.9898	0.9890
	LSTM	0.9964	0.9781	0.9965	0.9960
	TF	**0.9981**	**0.9851**	**0.9984**	**0.9981**

Tab. 4 presents an analysis of the performance of three models across four distinct waveform resampling tasks, utilizing Root Mean Square Error (RMSE), Mean Absolute Error (MAE), and Pearson Correlation Coefficient (PCC) as evaluative metrics. The TF performs best in all four tasks, achieving the lowest RMSE and the highest PCC. The TCN model has the highest overall error rate in all tests and its performance is relatively weakest among the three. It is worth noting that the square wave task poses the most severe challenge to all models. In summary, both qualitative (Fig. 5) and quantitative (Tab. 4) evidence suggests that it is reasonable to choose TF as the baseline model for this article.

B Feature Fusion

In the present paper, the feature fusion layer we used, as shown in Fig. 6, is based on a multi-scale attention aggregation (MSAA) module [8]. This feature fusion layer receives outputs from multiple attention mechanisms. It performs feature extraction and aggregation using the spatial attention mechanism on the left and the channel attention mechanism on the right. Finally, the results are fused through addition and 1D convolution.

Features from multiple attention mechanisms $X_1 \in \mathbb{R}^{C\times H\times W}$, $X_2 \in \mathbb{R}^{C\times H\times W}$,..., $X_N \in \mathbb{R}^{C\times H\times W}$ are spliced on the channel and then downscaled by 1-dimensional convolution, where the number of channels after convolution D is less than the number of channels before convolution C:

$$X \in \mathbb{R}^{D\times H\times W} = \text{Conv}(\text{Concat}(X_1, X_2, X_3)) \tag{5}$$

In the spatial attention mechanism, multi-scale fusion is achieved by concatenating and summing X through multiple convolutional layers with different convolutional kernel sizes:

$$X_1 \in \mathbb{R}^{D\times H\times W} = \text{Conv}_{3\times 3}(X) \tag{6}$$

$$X_2 \in \mathbb{R}^{D\times H\times W} = \text{Conv}_{5\times 5}(X) \tag{7}$$

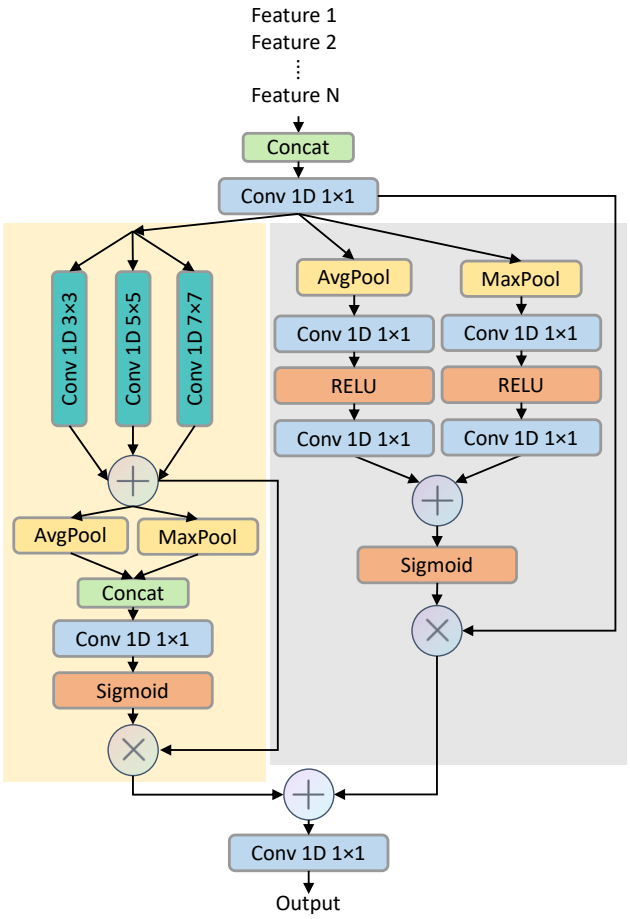

Figure 6: Feature Fusion.

$$X_3 \in \mathbb{R}^{D\times H\times W} = \text{Conv}_{7\times 7}(X) \tag{8}$$

$$S \in \mathbb{R}^{D\times H\times W} = X_1 + X_2 + X_3 \tag{9}$$

The output of the multi-scale fusion fed to average pooling and maximum pooling in the channel domain, followed by concatenation. It is then downscaled using a 1D convolution and generates spatial feature weights through sigmoid functions:

$$W_s \in \mathbb{R}^{1\times H\times W} = \text{Sigmoid}(\text{Conv}(\text{Pool}(S))) \tag{10}$$

The generated spatial feature weights W_s are then used to adjust the inputs to get the final spatial feature output:

$$O_s \in \mathbb{R}^{D\times H\times W} = W_s U \tag{11}$$

The channel attention on the right is used to adjust the channel weights of the input features. Given the input $X \in \mathbb{R}^{D\times H\times W}$, first the mean and maximum pooling in the spatial domain are performed to obtain the channel features respectively. The correlation between the channels is learned by two 1D convolutions and the channel weight representation is generated by the sigmoid function:

$$W_c \in \mathbb{R}^{D\times 1\times 1} = \text{Sigmoid}(\text{Conv}(\text{Conv}(\text{Pool}(X)))) \tag{12}$$

The generated channel feature weights W_c are then used to adjust the inputs to get the final channel feature output:

$$O_c \in \mathbb{R}^{D\times H\times W} = W_c X \tag{13}$$

The final channel feature output and the final channel feature output are summed and recovered by a 1D convolutional layer with the same number of channels as the input:

$$O \in \mathbb{R}^{C\times H\times W} = \text{Conv}(O_s + O_c) \tag{14}$$

The result is the fused feature.

C Loss Function

The following subsection introduces the loss functions employed in the training model phases of the present paper, except for the feature space loss. This paper aims to address the issue of time series upsampling. The sliding window is employed to handle extended sequences when computing the indicators, which necessitates sequences of uniform length. Although sliding windows may introduce additional losses, the requirements for model accuracy are not high during the training Phase 1. During the training Phases 2 and 3, the implemented feature space loss will rectify the inaccuracy induced by the sliding window.

- Mean Squared Error

$$\mathcal{L}_{\text{mse}} = \text{MSE}\left(\text{Window}(X_{\text{output}}), X_{\text{input}}\right) \tag{15}$$

  The objective of employing this loss is to ensure that the generated curve maintains an almost equal trend to the original series.

- Smoothness Loss

$$\mathcal{L}_{\text{smoothness}} = \text{Mean}\left(\left(\Delta^2(X_{\text{output}})\right)^2\right) \tag{16}$$

$$\Delta^2(X) = (x_{t+2} - x_{t+1}) - (x_{t+1} - x_t) \tag{17}$$

  The smoothness loss reduces the mean of the squares of the second-order differences, and pronounced fluctuations in the generated sequence can be efficiently mitigated, yielding a smoother curve.

- Gradient Loss

$$\mathcal{L}_{\text{gradient}} = \text{MSE}\left(\Delta\text{Window}(X_{\text{output}}), \Delta X_{\text{input}}\right) \tag{18}$$

$$\Delta(X) = (x_{t+1} - x_t) \tag{19}$$

  The gradient loss is used to ensure that the local change trend of the generated sequence closely matches that of the original sequence, while maintaining its critical characteristics.

D Significance Test

Tab. 5 and Tab. 6 are tables about statistical significance tests and performance differences. Batch training for this significance test is performed on a remote server equipped with 4x NVIDIA A100-40 GPUs and Intel Xeon Platinum 8368 CPU. These tests ensure that the observed performance differences are not accidental, but consistent. The data for these tests are derived from 12 independent model training samples. In the Tab. 5 and Tab. 6, the p-values less than 0.05 (i.e., statistically significant) are marked in green. For RMSE, when Diff is negative, the performance improves. For PCC, when Diff is positive, the performance improves. All performance improvements are highlighted in blue.

From Tab. 5, whether it is RMSE or PCC for three methods (CONV, S+C, S_C) and four datasets (WPuQ, PV-Live, Wind, MPVBench), Phase 2 and Phase 3 show statistically significant performance improvements compared to Phase 1. This can be clearly observed from the "Phase 2 vs. 1" and "Phase 3 vs. 1" rows: The vast majority of p-values are far below the 0.05 significance level, which indicates that these phase improvements are systematic effects. At the same time, these low p-values are accompanied by significant performance differences, e.g., the Diff of Phase 2 vs 1 for CONV method in the PCC part is generally 0.014 to 0.087. This broad and consistent improvement highlights the significant enhancement of model generalization ability and prediction accuracy brought about by the introduction of the discriminator.

Regarding the comparison between Phase 2 and Phase 3, although Phase 3 may exhibit a slight numerical advantage in some specific cases, the differences between the two phases are mostly not statistically significant in terms of p-values. This is reflected in the "Phase 3 vs. 2" row, where many p-values are not marked as red to indicate that they are less than 0.05 clearly. For example, in the S+C method of RMSE, the p-value of Phase 3 vs. 2 on the Train set of WPuQ is as high as 0.932, and the difference is 0.002. This indicates that, despite small performance fluctuations, the improvement in Phase 3 relative to Phase 2 is insufficient to be considered stable and reliable progress, and is likely due to random factors.

However, for the S_C method, Phase 3 showed significant performance changes compared to Phase 2. On the training sets, the performance of the S_C structure in Phase 3 was statistically significantly improved compared to Phase 2. For example, under the PCC indicator, the p-value of the WpuQ training set was 0.012, an increase of 0.024; under the RMSE indicator, the p-value of the WpuQ training set was 0.020, and the RMSE value decreased by 0.024. This indicates that Phase 3 yielded significant optimization effects on the S_C structure during the training phase. Despite the excellent performance on the training set, the improvement of the S_C structure in Phase 3 compared to Phase 2 was mostly not statistically significant on the test set. For example, under the PCC indicator, the p-value on the WPuQ

test set is 0.913, with a difference of only 0.003; under the RMSE indicator, the p-value on the WPuQ test set is 0.961, with a difference of -0.002, which is in sharp contrast to the significant improvement on the training set, indicating that the S_C structure's robustness and generalization ability on actual unseen data need to be strengthened.

From Tab. 6, from the RMSE and PCC indicator, the structure containing convolution (CONV) is significantly better than the structure containing only self-attention (SELF). In almost all datasets (WPuQ, PV-Live, Wind, MPVBench) and all phases (Phase 1, Phase 2, Phase 3), the p-values of the structure containing CONV vs. SELF are near 0.000. The Diff value is positive for PCC and negative for RMSE, indicating that the CONV structure has a significant performance improvement compared to the SELF structure.

However, when CONV, S_C and S+C are compared with each other, their performance is relatively close. In terms of training set fitting, S_C only shows a statistically significant advantage over CONV and S+C on the Wind and MPVBench datasets, but not on the WPuQ and PV-Live datasets. It is worth emphasizing that in the Phase 3 training set, the S_C structure significantly outperforms the CONV and S+C structures on multiple datasets (such as WPuQ and MPVBench). For example, in the PCC indicator of the WPuQ training set, the p-value of S_C vs CONV is 0.003, the p-value of S_C vs S+C is 0.001, and the Diff values are all positive; in the RMSE indicator of the MPVBench training set, the p-values of S_C vs CONV and S_C vs S+C are both close to 0.000. The Diff values are all negative, showing a significant improvement of S_C. This shows that the S_C structure has a stronger ability to learn known data features and perform super-resolution processing on them. In terms of generalization ability on the test set, S_C fails to show a statistically significant advantage over both CONV and S+C, although it has an average performance improvement on some datasets. Since the real high-resolution dataset is not directly used to calculate the loss during training, the performance on the training set should not be attributed to overfitting. It more reflects that the model learns to generate outputs that are highly close to the real data during training, but its ability to accurately match unseen inputs is weakened.

In general, the introduction of discriminator and CONV has significantly improved the performance of the TF. However, among different method combinations (such as CONV, S+C, S_C), it is difficult to draw a unified conclusion to prove that a certain combination has a generally significant performance improvement over other combinations. The S_C method is better than other methods in numerical performance in the training set, but the improvement in test set is relatively limited.

It is worth noting that although S_C shows better fitting ability on the training set, the gap with other methods in the generalization performance of the test set is narrowed, and the statistical significance is limited. This may be attributed to:

- The differences in the characteristics of different datasets affect the relative performance of the methods.
- The current experimental scale may not be sufficient to fully distinguish subtle method differences.

However, since this paper primarily addresses the problem of time series upsampling and SR, achieving better results on the training set alone may be preferable in certain scenarios, such as data preprocessing steps.

Table 5: Phase Comparison - Statistical Significance Tests and Performance Differences

				WPuQ				**PV-Live**				**Wind**				**MPVBench**			
				Train		Test		Train		Test		Train		Test		Train		Test	
				P-Val	Diff	P-Val	Diff	P-Val	Diff	P-Val	Diff	P-Val	Diff	P-Val	Diff	P-Val	Diff	P-Val	Diff
PCC	CONV	Phase 2	Phase 1	0.000	0.087	0.000	0.072	0.000	0.046	0.000	0.046	0.000	0.014	0.000	0.014	0.013	0.026	0.018	0.025
		Phase 3	Phase 1	0.000	0.085	0.000	0.057	0.000	0.047	0.000	0.046	0.000	0.016	0.000	0.014	0.008	0.028	0.020	0.025
			Phase 2	0.772	-0.002	0.000	-0.015	0.000	0.001	0.929	0.000	0.000	0.002	0.998	0.000	0.000	0.002	0.317	0.000
	SELF	Phase 2	Phase 1	0.014	-0.007	0.000	-0.012	0.160	0.004	0.022	0.006	0.000	0.006	0.000	0.010	0.259	0.003	0.129	0.004
		Phase 3	Phase 1	0.000	-0.009	0.000	-0.017	0.005	0.005	0.000	0.007	0.437	0.002	0.056	0.004	0.554	0.001	0.624	0.001
			Phase 2	0.425	-0.003	0.109	-0.005	0.723	0.002	0.692	0.002	0.039	-0.005	0.008	-0.006	0.559	-0.002	0.330	-0.003
	S+C	Phase 2	Phase 1	0.000	0.080	0.000	0.071	0.000	0.048	0.000	0.049	0.000	0.015	0.000	0.014	0.000	0.016	0.000	0.015
		Phase 3	Phase 1	0.000	0.079	0.000	0.062	0.000	0.049	0.000	0.049	0.000	0.017	0.000	0.014	0.000	0.018	0.000	0.015
			Phase 2	0.989	-0.001	0.187	-0.009	0.000	0.001	0.581	0.000	0.000	0.002	0.593	0.000	0.000	0.002	0.049	-0.001
	S_C	Phase 2	Phase 1	0.000	0.062	0.000	0.043	0.000	0.060	0.000	0.060	0.000	0.013	0.000	0.011	0.000	0.025	0.000	0.023
		Phase 3	Phase 1	0.000	0.085	0.000	0.046	0.000	0.061	0.000	0.060	0.000	0.016	0.000	0.011	0.000	0.028	0.000	0.023
			Phase 2	0.012	0.024	0.913	0.003	0.000	0.001	0.918	0.000	0.000	0.003	0.197	-0.001	0.000	0.003	0.088	-0.001
RMSE	CONV	Phase 2	Phase 1	0.000	-0.076	0.000	-0.061	0.000	-0.098	0.000	-0.095	0.000	-0.034	0.000	-0.028	0.002	-0.052	0.003	-0.051
		Phase 3	Phase 1	0.000	-0.071	0.000	-0.043	0.000	-0.101	0.000	-0.095	0.000	-0.039	0.000	-0.028	0.001	-0.058	0.003	-0.051
			Phase 2	0.208	0.005	0.000	0.018	0.000	-0.003	0.989	0.000	0.000	-0.005	0.860	0.000	0.000	-0.006	0.817	0.000
	SELF	Phase 2	Phase 1	0.004	0.009	0.000	0.012	0.287	-0.004	0.097	-0.005	0.000	-0.007	0.000	-0.009	0.228	-0.002	0.115	-0.003
		Phase 3	Phase 1	0.000	0.011	0.000	0.015	0.000	-0.006	0.000	-0.008	0.190	-0.003	0.029	-0.004	0.357	-0.001	0.443	-0.001
			Phase 2	0.871	0.001	0.425	0.003	0.570	-0.002	0.524	-0.002	0.059	0.004	0.012	0.005	0.613	0.001	0.378	0.002
	S+C	Phase 2	Phase 1	0.000	-0.068	0.000	-0.058	0.000	-0.101	0.000	-0.100	0.000	-0.034	0.000	-0.027	0.000	-0.040	0.000	-0.039
		Phase 3	Phase 1	0.000	-0.066	0.000	-0.048	0.000	-0.103	0.000	-0.099	0.000	-0.039	0.000	-0.026	0.000	-0.045	0.000	-0.038
			Phase 2	0.932	0.002	0.100	0.010	0.001	-0.002	0.566	0.001	0.000	-0.005	0.773	0.001	0.000	-0.005	0.101	0.002
	S_C	Phase 2	Phase 1	0.000	-0.063	0.000	-0.043	0.000	-0.121	0.000	-0.118	0.000	-0.030	0.000	-0.022	0.000	-0.054	0.000	-0.051
		Phase 3	Phase 1	0.000	-0.087	0.000	-0.045	0.000	-0.125	0.000	-0.117	0.000	-0.039	0.000	-0.021	0.000	-0.063	0.000	-0.049
			Phase 2	0.020	-0.024	0.961	-0.002	0.000	-0.004	0.833	0.000	0.000	-0.009	0.186	0.002	0.000	-0.009	0.106	0.002

Table 6: Method Comparison - Statistical Significance Tests and Performance Differences

				WPuQ				PV-Live				Wind				MPVBench			
				Train		Test		Train		Test		Train		Test		Train		Test	
				P-Val	Diff	P-Val	Diff	P-Val	Diff	P-Val	Diff	P-Val	Diff	P-Val	Diff	P-Val	Diff	P-Val	Diff
PCC	Phase 2	CONV	Gauss	0.000	0.051	0.000	0.032	0.000	0.000	0.002	0.000	0.000	0.002	0.602	0.000	0.001	0.000	0.036	0.000
			SELF	0.000	0.116	0.000	0.110	0.000	0.178	0.000	0.177	0.000	0.118	0.000	0.121	0.000	0.170	0.000	0.172
		Gauss	SELF	0.000	0.066	0.000	0.078	0.000	0.178	0.000	0.177	0.000	0.116	0.000	0.121	0.000	0.170	0.000	0.172
		S+C	CONV	0.282	-0.009	0.744	-0.004	0.368	0.000	0.299	0.000	0.990	0.000	0.993	0.000	0.997	0.000	0.856	0.000
			Gauss	0.000	0.041	0.000	0.028	0.000	0.000	0.000	0.000	0.000	0.002	0.259	-0.001	0.002	0.000	0.012	0.000
			SELF	0.000	0.107	0.000	0.106	0.000	0.178	0.000	0.177	0.000	0.118	0.000	0.121	0.000	0.170	0.000	0.172
		S_C	CONV	1.000	0.001	1.000	0.001	0.999	0.000	0.999	0.000	0.884	0.000	0.305	0.001	0.004	0.001	0.993	0.000
			Gauss	0.000	0.052	0.000	0.032	0.000	0.000	0.029	0.000	0.000	0.002	0.664	0.000	0.000	0.001	0.015	0.000
			SELF	0.000	0.117	0.000	0.110	0.000	0.178	0.000	0.177	0.000	0.119	0.000	0.122	0.000	0.171	0.000	0.172
			S+C	0.515	0.010	0.903	0.004	0.287	0.000	0.303	0.000	0.983	0.000	0.119	0.001	0.007	0.001	0.580	0.000
	Phase 3	CONV	Gauss	0.000	0.049	0.000	0.016	0.000	0.001	0.674	0.000	0.000	0.004	0.825	0.000	0.000	0.002	0.022	-0.001
			SELF	0.000	0.117	0.000	0.099	0.000	0.178	0.000	0.175	0.000	0.125	0.000	0.127	0.000	0.174	0.000	0.174
		Gauss	SELF	0.000	0.068	0.000	0.083	0.000	0.176	0.000	0.175	0.000	0.121	0.000	0.127	0.000	0.172	0.000	0.175
		S+C	CONV	0.633	-0.008	0.972	0.003	0.782	0.000	1.000	0.000	0.990	0.000	0.734	-0.001	0.999	0.000	1.000	0.000
			Gauss	0.000	0.040	0.005	0.019	0.000	0.001	0.941	0.000	0.000	0.004	0.073	-0.001	0.000	0.002	0.010	-0.001
			SELF	0.000	0.109	0.000	0.102	0.000	0.177	0.000	0.175	0.000	0.125	0.000	0.126	0.000	0.174	0.000	0.174
		S_C	CONV	0.003	0.027	0.030	0.018	0.076	0.000	0.999	0.000	0.035	0.002	0.996	0.000	0.000	0.002	0.842	0.000
			Gauss	0.000	0.075	0.000	0.035	0.000	0.002	0.996	0.000	0.000	0.005	0.668	-0.001	0.000	0.004	0.005	-0.001
			SELF	0.000	0.143	0.000	0.118	0.000	0.178	0.000	0.175	0.000	0.126	0.000	0.127	0.000	0.176	0.000	0.174
			S+C	0.001	0.035	0.152	0.016	0.011	0.001	1.000	0.000	0.062	0.002	0.945	0.000	0.000	0.002	0.887	0.000
RMSE	Phase 2	CONV	Gauss	0.000	-0.047	0.000	-0.028	0.003	-0.001	0.714	0.000	0.001	-0.004	0.223	0.001	0.311	-0.001	0.021	0.002
			SELF	0.000	-0.099	0.000	-0.089	0.000	-0.239	0.000	-0.233	0.000	-0.175	0.000	-0.157	0.000	-0.199	0.000	-0.202
		Gauss	SELF	0.000	-0.051	0.000	-0.061	0.000	-0.238	0.000	-0.233	0.000	-0.171	0.000	-0.158	0.000	-0.198	0.000	-0.204
		S+C	CONV	0.252	0.009	0.708	0.004	0.197	0.000	0.150	-0.001	0.993	0.000	0.999	0.000	0.914	0.000	0.759	-0.001
			Gauss	0.000	-0.038	0.000	-0.025	0.000	-0.001	0.009	-0.001	0.000	-0.004	0.133	0.002	0.024	-0.001	0.009	0.001
			SELF	0.000	-0.090	0.000	-0.086	0.000	-0.240	0.000	-0.234	0.000	-0.176	0.000	-0.156	0.000	-0.199	0.000	-0.203
		S_C	CONV	0.999	-0.001	1.000	0.000	0.933	0.000	0.985	0.000	0.621	-0.001	0.191	-0.002	0.004	-0.003	0.999	0.000
			Gauss	0.000	-0.049	0.000	-0.029	0.000	-0.001	0.398	0.000	0.000	-0.005	0.923	0.000	0.001	-0.003	0.008	0.002
			SELF	0.000	-0.100	0.000	-0.090	0.000	-0.239	0.000	-0.233	0.000	-0.177	0.000	-0.158	0.000	-0.202	0.000	-0.203
			S+C	0.472	-0.011	0.914	-0.004	0.342	0.000	0.386	0.000	0.858	-0.001	0.115	-0.002	0.011	-0.002	0.826	0.000
	Phase 3	CONV	Gauss	0.000	-0.042	0.000	-0.011	0.000	-0.004	0.996	0.000	0.000	-0.009	0.738	0.001	0.000	-0.007	0.014	0.002
			SELF	0.000	-0.095	0.000	-0.074	0.000	-0.240	0.000	-0.231	0.000	-0.185	0.000	-0.162	0.000	-0.206	0.000	-0.204
		Gauss	SELF	0.000	-0.053	0.000	-0.064	0.000	-0.236	0.000	-0.231	0.000	-0.176	0.000	-0.163	0.000	-0.200	0.000	-0.206
		S+C	CONV	0.803	0.006	0.814	-0.004	0.842	0.001	1.000	0.000	0.999	0.000	0.647	0.001	0.980	0.001	0.985	0.000
			Gauss	0.000	-0.036	0.016	-0.015	0.000	-0.003	1.000	0.000	0.000	-0.009	0.044	0.002	0.000	-0.006	0.010	0.003
			SELF	0.000	-0.088	0.000	-0.079	0.000	-0.239	0.000	-0.231	0.000	-0.185	0.000	-0.161	0.000	-0.206	0.000	-0.203
		S_C	CONV	0.004	-0.031	0.027	-0.020	0.060	-0.002	0.998	0.000	0.040	-0.005	0.987	0.001	0.000	-0.005	0.699	0.001
			Gauss	0.000	-0.073	0.001	-0.031	0.000	-0.005	1.000	0.000	0.000	-0.014	0.495	0.001	0.000	-0.012	0.005	0.003
			SELF	0.000	-0.126	0.000	-0.094	0.000	-0.241	0.000	-0.230	0.000	-0.190	0.000	-0.162	0.000	-0.211	0.000	-0.203
			S+C	0.002	-0.037	0.177	-0.016	0.015	-0.002	0.999	0.000	0.048	-0.004	0.945	-0.001	0.000	-0.006	0.933	0.001